Journal of Operation and Automation in Power Engineering

Vol. 14, No. 3, Aug. 2026, Pages: 198-208

http://joape.uma.ac.ir

Research Paper

A New Fast and Accurate Method Based on Fourier Transform for Fault Detection in DC Microgrids

Mohammad Kohzadipour , *Majid Valizadeh* * , *Sabah Daniar* , and *Amirhosein Khosaravi Sarvenoee*

Department of Electrical Engineering, Ilam University, Ilam, Iran.

Abstract— *This paper utilizes the Fast Fourier Transform (FFT) technique to extract the apparent power of DC microgrids for fault detection. The proposed method separates the real and imaginary components of power and compares the imaginary part with a predetermined threshold. To determine the relay threshold, PP and PG faults are simulated at various distances along each line connected to each bus. The Inverse Fast Fourier Transform (IFFT) is then calculated for each fault at each line and location. The relay threshold is selected based on the lowest significant value among the highest IFFT values calculated for all microgrid lines. This study proposes a novel relay threshold calculation approach, enabling precise fault detection and localization in DC microgrids. The relay threshold value is calculated at the control center and then sent to the microgrid relays. Fault detection is achieved by comparing the IFFT values obtained within the microgrid with the relay threshold value. Once the relay threshold is surpassed, the microgrid detects the fault and promptly sends a trip signal to the circuit breaker. This fault detection strategy accurately identifies the fault location by measuring the current and voltage between the terminals of the faulty section. The proposed method swiftly detects all PP and PG faults (including HIF up to 50 ohms) in grid-connected and islanded modes within 2-3 milliseconds. It accurately locates faults with minimal deviation across various positions. Rigorous simulations using MATLAB and EMTP-RV programs confirm the effectiveness of the protection scheme, emphasizing its reliable performance.*

Keywords—DC microgrid, energy threshold, fault detection, fault location, inverse fast fourier transform, protection.

NOMENCLATURE

Symbols

AIDM	Adaptive Islanding Detection Method
ALPSO	Augmented Lagrangian Particle Swarm Optimization
ALT	Advanced Learning Technique
CCNG	DC Nano-Grids
CNN	Convolutional Neural Network
CS	Compressed Sensing
DCMG	DC Microgrid
DCNG	DC Nano-Grids
DNN	Deep Neural Networks
DWT	Discrete Wavelet Transform
EMD	Empirical Mode Decomposition
ESS	Energy Storage Source
EV	Electric Vehicle
FDIA	False Data Injection Attacks
FDLC	Fault Detection, Location, and Classification
FDM	Fault Detection Method
FFT	Fast Fourier Transform
FSSTH	High-Order Synchro Squeezing Transform
HHT	Hilbert-Huang Transform
HIF	High-Impedance Faults
IFFT	Imaginary Fast Fourier Transform
IMF	Intrinsic Mode Functions
KNN	K-Nearest Neighbor
LSTM	Long Short-Term Memory
MAF	Moving Average Filter
MM	Mathematical Morphology
MODWPT	Maximum Overlap Discrete Wavelet Packet Transform
MPPT	Maximum Power Point Tracking
MRA	Multiresolution Analysis
PCC	Point of Common Coupling
PCM	Power Control Mechanism
PEA	Phasor Estimation Algorithm
PG	Pole to Ground
POC	Passive Oscillators
PP	Pole to Pole
PPU	Probing Power Unit
PSO	Particle Swarm Optimization
PV	Photovoltaic
PWM	Pulse Width Modulation
RT	Regression Trees
SDFT	Sliding Window Discrete Fourier Transform
STFT	Short-Time Fourier Transform
SVD	Singular Value Decomposition
SVM	Support Vector Machines
TSA	Time Synchronization Algorithm
TW	Traveling Waves

Received: 16 Sept. 2024
Revised: 21 Jan. 2025
Accepted: 27 Jan. 2025
*Corresponding author:
E-mail: m.valizadeh@ilam.ac.ir (M. Valizadeh)
DOI: 10.22098/joape.2025.15858.2218

1. INTRODUCTION

Considering the rapid integration of renewable energy sources such as PV panels and wind energy, along with the increasing use of Energy Storage Systems (ESS), DC microgrids have been identified as a viable solution for modern distribution systems. These microgrids offer increased efficiency, reduced losses, and simpler integration with direct current-based resources, making them an optimal platform for distributed generation sources. However, as these systems grow in complexity, ensuring their reliability and resilience against failures presents a significant challenge [1–4]. Fault detection in DC microgrids is a significant challenge in today's power systems. Unlike AC systems, which have optimized fault detection mechanisms, DC systems face challenges due to the absence of such mechanisms and fundamental differences in electrical behavior. This is especially crucial in DC microgrids with DG sources and DC loads, where high fault currents from LIF and HIF can damage power converters, batteries, and sensitive equipment. Failure to detect faults quickly can lead to system instability, power outages, and equipment destruction. Therefore, developing innovative and rapid fault detection methods for DC microgrids is essential. These methods should accurately identify various types of faults, including those with variable impedance and in different environmental conditions. Using Fourier transform as a signal analysis tool can significantly improve fault detection accuracy and speed. This technique allows for precise analysis of frequency components in current and voltage signals. Extensive research has been conducted to design efficient protective systems in DC microgrids to enhance reliability and stability while minimizing equipment damage [5–8].

1.1. Literature review

This paper [9] introduces a domain transformation-based fault detection method for DC microgrids that maintains stable performance under various microgrid conditions. Various faults were simulated using a Matlab/Simulink model of a grid-connected DC microgrid, including photovoltaic systems and battery storage. Short-Time Fourier Transform (STFT) is applied to error time signals to obtain the frequency spectrum. The selected features from the frequency spectrum are then presented to several intelligent classifiers. This study [10] proposes a new protective algorithm based on traveling waves (TWs) for fault detection and location. In this method, Fast S-Transform with Hilbert-Huang Transform (FSSTH) is used for the precise identification of traveling waves at the relay location. FSSTH improves the accuracy and speed of fault detection by providing a more precise time-frequency representation. This method can accurately identify transient phenomena such as traveling waves in DC microgrids even in the presence of noise and variable fault resistance. Using the spectral chamber and FSSTH, tracking regions in the time-frequency domain are extracted, which improves fault detection. This approach also distinguishes between internal and external errors by evaluating the polarization of traveling waves and identifies the direction of the fault.

In order to properly identify different kinds of short-circuit defects in power systems, this study [11] suggests a data preprocessing technique that could lead to more efficient power repair and maintenance procedures. The proposed technique involves creating a time-frequency energy map by using the Short-Time Fourier Transform (STFT) to convert the observed voltage and current signals into the time and frequency domains. To categorize the short-circuit defects, a Convolutional Neural Network (CNN) is then trained and evaluated to classify short-circuit defects. In this research, an approach to determine the decision of microgrid islanding is also proposed. This methodology [12] consists of two phases: feature extraction and categorization. During the feature extraction process, the symmetrical components of voltage, current, and the product of voltage and current of the second-order harmonic are obtained by processing real-time three-phase voltage and current observations using a discrete Fourier transform.

The second step is based on a machine learning method known as the KNN approach, using the nine retrieved attributes as inputs. In order to identify the fault site in DC micro-grids, this project [13] proposes a technique based on PSO and compares its results with the least-squares approach. This technique locates the issue by utilizing a PPU in DC micro-grids, where the damping resonant frequency and attenuation constant determine the distance of the fault from the PPU. The suggested PSO-based technique determines the attenuation constant, while the FFT provides the damping resonant frequency of the fault current. A smart FDM for MGs based on DNNs and the HHT is presented [14].

To safeguard MGs and restore services, the proposed scheme aims to quickly detect the type, phase, and location of faults. Singular Value Decomposition (SVD) is used to extract specific features from Intrinsic Mode Function (IMFs) obtained from Hilbert-Huang Transform (HHT) to serve as input for Deep Neural Networks (DNNs). The HHT processes the branch current measurements gathered from protective relays in order to extract relevant characteristics. In [15], a new approach to fault classification and detection in a renewable microgrid is introduced. The main contributions focus on two key areas. Firstly, enhancing fault detection performance in microgrids with nonlinear interactions, such as varying electric loads, hydrokinetic, and solar systems. Secondly, a robust method for fault identification and classification is presented by combining Discrete Wavelet Transform various neural networks and supervised learning techniques. This paper [16] presents the FDLC method in a solar DCMG. This microgrid consists of two DCNGs with a PCM. The FDLC method utilizes a voltage circuit with a sensor and a diode network for fault detection, employing six expressions derived from line-to-line and line-to-ground fault analysis in microgrids. In this research [17], an advanced method for detecting DC arc faults in DC microgrids has been introduced. This method is based on the variances in features within moving windows and the use of ALTs. The signal obtained from the power supply signals is utilized as the reference input for the model. A TW-based method for fast protection in DC microgrids has been introduced in [18]. The DWT is employed to calculate the high-frequency components of fault currents in the DC system. MRA is used to identify moving wave components at different frequencies. The Parsval energy of the MRA coefficients is calculated to establish a quantitative relationship between the energy of the flow error signal and the energy of their coefficients. A new local current-based method for the rapid detection of HIF in DC microgrid clusters using MM has been introduced in [19]. The proposed strategy consists of two MM-based components: the first part involves MM erosion filtering to extract flow signals and their components for differential feature extraction.

The second part of the MM regional maxima is utilized to determine a critical value for quickly identifying faults in line sections. A method has been introduced for estimating resistance and identifying faults in situations where high-resistance faults are present. Resistance is estimated through local measurements at the stations, and then its polarity at both ends of the line section is compared to pinpoint the fault. By utilizing the resistance marker, timing synchronization issues are eliminated. This method is capable of detecting faults in DC microgrids with both radial and loop configurations [20]. A DC fault detection technique has been introduced in [21] to enhance the protection of DC microgrid clusters. Empirical mode decomposition and the Hilbert transform are utilized for quick and accurate error identification. The rapid increase of fault currents in DC systems creates serious time constraints for fault isolation posing a significant challenge for DC microgrid protection. Additionally, high-impedance faults in DC systems can lead to minor changes in current that, if not detected promptly, can result in damage to power electronic converters. A DC microgrid integrated with PV panels, modeled

on the MATLAB/Simulink platform, has been introduced in [22] for fault detection and classification on both AC and DC sides. DC signals are extracted from the DC bus terminals of the DC microgrid system to analyze the proposed system's results. To enhance the system's response speed, derivatives of DC current signals (dIdc/dt) are used, focusing on non-static and nonlinear characteristics, including local fractal components that may create complex issues in the system.

This paper [23] presents an accurate method for identifying the first fault in IT earthing systems. In this method, the AC component along with the SDFT is used to estimate the error impedance. The high accuracy of this process is achieved due to the severe filtering with the implicit MAF. Additionally, by using dual search tables and the Goertzel algorithm in SDFT, further computational savings are achieved. The aim of this project [24] is to develop fast and reliable methods for fault detection and location in DC microgrids to enhance operational efficiency, reduce environmental impacts, and achieve resource conservation and sustainability goals. The error detection method uses CS techniques and RT. A precise method for error localization has also been introduced by combining the feature matrix and the LSTM model. This study [25] proposes an intelligent method for fault detection and classification in microgrids. This method is performed by combining three different computational tools: signal processing through the MODWPT, parameter optimization using ALPSO, and machine learning using SVM. MODWPT is used for preprocessing post-fault currents at both ends of the feeders. This paper [26] proposes an innovative method for fault detection and localization in a mesh configuration DC microgrid. The proposed method is based on analyzing the similarity between the flow of sampled lines and the flow of reference lines using the improved Pearson correlation coefficient. Initially, error detection is performed by comparing the sampled line currents with the fixed line currents within a sliding time window. Then, the type and location of the error are identified by analyzing the correlation coefficient. In the next step, the fault location is determined by comparing the sampled line currents with the computed results of the transient line currents related to the estimated fault location in a fixed time window. A new algorithm has been presented in [27] for Phasor Estimation Algorithm (PEA) under fault conditions for MG applications. The main features of this method include accurate estimation of the signal phasor, which consists of a decreasing DC component, a decreasing main component with the fundamental frequency, and harmonics. In this strategy, the Taylor series is replaced with exponential functions of the main frequency and a decreasing DC component. The time constants and the values of the damping components are estimated using the least squares method. The project [28] initially examines coordinated attacks that involve multiple False Data Injection Attacks (FDIA) or Time Synchronization Attacks (TSA). These attacks are executed almost simultaneously and independently to achieve a specific goal, posing potential threats to MG. A case study illustrates how these coordinated attacks can trigger a chain of events that lead to instability in the entire microgrid. A method for identifying these attacks and distinguishing them from real errors is proposed, involving the use of POCs that are placed in series with each converter. This paper [29] proposes a microgrid islanding detection method designed to overcome the limitations of both passive and traditional active detection methods.

Traditional passive detection methods often struggle with accurately setting fault thresholds, while active methods can have a negative impact on power quality. To address these issues, the proposed method combines the SDFT and EMD with an LSTM network optimized by an attention mechanism. In this approach, the inverter's output current and voltage at the PCC are processed using the SDFT to enhance detection accuracy and reliability. In this research [30], an AIDM in AC/DC hybrid microgrid networks has been presented. This method, which utilizes a combination of artificial intelligence and signal processing, is designed to distinguish between different error and disturbance conditions that lead to islanding or non-islanding states. To detect islanding and non-islanding conditions, disturbance/error signals are first received and analyzed from a test microgrid. Table 1 compares the proposed method with other existing methods.

1.2. Important features of the article

The main advantages of this paper's work lie in the use of a combination of FFT and IFFT for fault detection and localization in DC microgrids, which include the following features:

- **Quick and accurate fault detection:** This method is capable of identifying HIF and LIF in less than 3 milliseconds, which is much faster than many existing methods.
- **Topology-independent microgrid operation:** The proposed method maintains its performance even under conditions of microgrid topology change (such as switching from grid-connected mode to island mode).
- **Covering various types of faults:** This method has the capability to detect PP and PG faults, both of which are common types of faults in DC microgrids.
- **Simplification in threshold calculations:** The threshold value is calculated offline through the analysis of simulated errors and transferred to the relays, which reduces the need for complex real-time computations.

These advantages make the proposed method superior to other existing approaches in fault detection in DC microgrids and give it a high potential for practical implementation.

In light of the existing protection strategies delineated thus far, a multitude of methodologies have been proposed for fault detection and localization. However, these methods present significant conservation challenges, underscoring the imperative of addressing and comparing them with the proposed conservation scheme.

A significant deficiency observed in existing methods lies in their oversight of High Impedance faults within DC microgrids. These faults, prevalent in such grids, pose a distinct challenge due to their characteristic slow rise in fault current levels compared to Low Impedance faults. Failure to promptly identify HIFs not only jeopardizes network stability but also compromises the safety of individuals reliant on the grid. Moreover, transitioning microgrid operation modes between On-Grid and Off-Grid configurations presents an additional hurdle for protection mechanisms. The distinct fault current profiles in these topologies render fixed threshold values inadequate for comprehensive fault detection and identification. Furthermore, many current methodologies fall short of distinguishing the precise fault location within the microgrid. To address these critical gaps, this research introduces a comprehensive protection scheme offering the following capabilities: detection of PP and PG faults, robust operation and fault identification in both On-Grid and Off-Grid scenarios, detection of both LIF and HIF up to a fault resistance of 50Ω across all network operation modes, immunity to changes in microgrid topology, fault localization capability in both fault types, and swift fault detection within two to three milliseconds irrespective of microgrid operation mode.

2. Proposed Method

In this section, the proposed method will be explained in detail. Additionally, it will include the structure of the DC microgrid, photovoltaic system, DC-DC boost converter, protective method, threshold value calculation, relay algorithm, and fault location.

2.1. DC microgrid architecture

In order to operate in two modes, connected and disconnected from the grid, a microgrid with photovoltaic sources must be equipped with an energy storage device, such as a battery. Since there are typically both DC and AC loads in a network, the overall structure of the analyzed network will be as shown in Fig. 1.

Table 1. Analysis of conventional DC microgrid protection methods.

Ref.	Protection strategy	Advantages	Disadvantages	Research gaps
[9]	Frequency patterns of faults in short time periods	Stability in microgrid changes	High processing complexity	Fault detection under conditions of varying power, load and changing current direction
[10]	Traveling wave analysis and time-frequency tracking	Robustness to noise and variable resistance	Computational complexity	Fault detection and localization in the presence of noise, topology changes, and high-resistance faults
[11]	Time-frequency analysis and CNN	High performance	Need to fine-tune the model	Performance at different load levels and various system scenarios, reducing model training time
[12]	Fourier + ML for isolation detection	High isolation detection accuracy	Sensitive to noise	Review of three-phase and single-phase faults, mismatch of active and reactive powers
[13]	FFT + PSO	High fault location accuracy	Needs accurate data	Lower sampling rate compared to the travel wave (TW) method
[14]	DNN + HHT	Real-time performance	High computational complexity	Compare identification fault type and location with other method
[15]	DWT + supervised learning	Automatic learning	High computational complexity	Ability to detect high impedance faults
[16]	Fault detection and classification	Simple and low cost	Needs calibration	The ability to distinguish between LG and LL faults from partial shadow conditions
[17]	Advanced diagnostics	Increased efficiency	Implementation complexity	Minimizing the impacts of system noise
[18]	Traveling wave + DWT	Frequency domain analysis	Sensitive to system changes	Analysis communication infrastructure
[19]	Mathematical Morphology	Increased accuracy	Computational complexity	The ability to accurately extract signals without distortion by MM
[20]	Resistance estimation	Accurate resistance estimation	Sensitive to parameter changes	Proper performance for close faults, noise conditions, and load changes
[21]	Fast and accurate identification	High accuracy	Complex calculations	Identify high impedance faults, communication channel, reduction costs and increasing speed
[22]	DC derivatives + fractal analysis	Accurate classification	Non-linear, non-static nature	Signal decomposition techniques, resulting in a reduction in computational load
[23]	AC injection + SDFT	Saves computation	Limited conditions	The accuracy of the proposed method is due to the use of the Moving Average Filter (MAF)
[24]	Fast fault ID and location	High precision	Computational complexity	Reducing the sampling rate, threshold value elimination
[25]	MODWPT	Efficient system response	Dependent on signals	Higher immunity against noise and disturbances in the MODWPT system compared to DWT
[26]	Improved Pearson correlation	Simple approach	Depends on fault conditions	Identification accuracy of the faulty line, fault resistance value, and fault location under various conditions
[27]	Parameter Estimation Algorithm	High accuracy	Sensitive parameters	Estimating signals due to asymmetry, harmonics, and DC signals components during transient periods and faults
[28]	Power Oscillation Control (POC)	Detect coordinated attacks	High cost	Network configuration, sensitivity to high-resistance faults, the ability to distinguish between cyber-attacks and common network faults
[29]	SDFT + EMD	Improved accuracy	High computational load	Resistance to noise, differentiation between islanding and non-islanding conditions of the network
[30]	Adaptive Islanding Detection (AIDM)	High versatility	High computational complexity	Distinguish between island and non-island states with high accuracy and reliability
This Paper	FFT + IFFT	High accuracy in fault detection	—	-

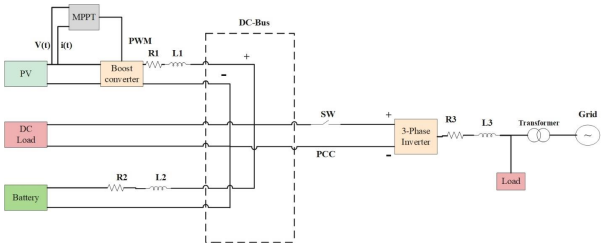

Fig. 1. General schematic of the studied DC microgrid.

Additionally, Fig. 2 displays the Maximum Power Point tracking (MPPT) by Perturb and Observe (P and O) method for maximizing photovoltaic power [31].

Furthermore, in this architecture, the DC microgrid is connected to its upstream grid through the SW switch at the PCC point, which can operate both On-Grid and Off-Grid. Microgrids in Off-Grid mode are powered by renewable energy sources, such as a photovoltaic system, and batteries. When the microgrid is operating in On-Grid mode, the power grid can supply DC load power [31].

2.2. Photovoltaic system

As shown in Fig. 3, the equivalent circuit of the DC microgrid photovoltaic system includes a controlled current source, a parallel diode, and series and parallel resistors.

When exposed to sunlight, solar cells generate DC voltage through P-N semiconductor junctions. The following mathematical relationships can be used to calculate the current and voltage of a solar cell:

$$I_{PV} = I_L - I_O\left(e^{\frac{q(V_{PV}-I_{PV}R_s)}{nkT}} - 1\right) - \frac{V_{PV}+I_{PV}R_s}{R_{sh}} \quad (1)$$

$$V_{PV} = \frac{N_s nkT}{q}\ln\left(\frac{I_{sc}+K_I(T-T_{ref})G+I_O-I_{PV}+N_P}{I_O N_P}\right) - \frac{N_s}{N_P}R_S I_{PV} \quad (2)$$

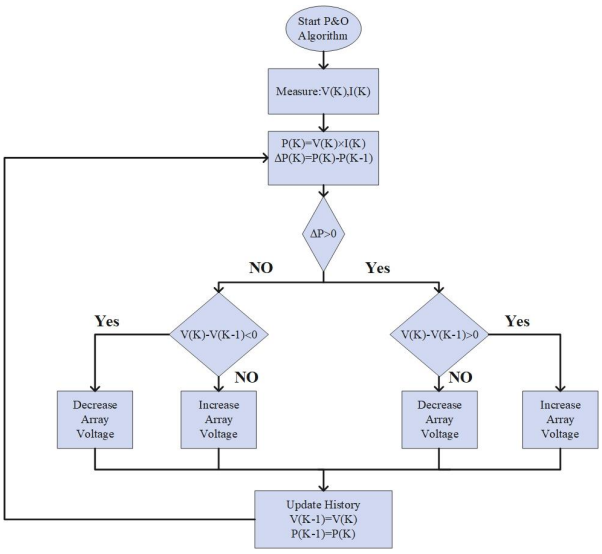

Fig. 2. P and O method performance algorithm used in MPPT control system.

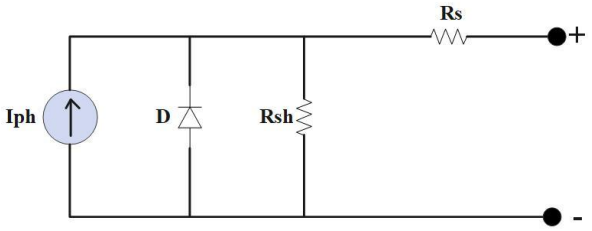

Fig. 3. Solar cell equivalent circuit.

In these relationships, I_{PV} represents the current of solar cells, I_L is the produced light, and I_O is the current of the diode. additionally, n, q and k are the ideal diode coefficient, electron charge and Boltzmann's constant, respectively. The value of Boltzmann's constant is $1/3805 \times 10^{(-23)}$J/K. R_S is the series resistance of the solar cell and R_{sh} is the shunt resistance of the solar cell. Also, N_s is the number of connected series cells and N_p is the number of parallel cells in the solar system [31].

2.3. DC-DC boost converter

To increase the voltage level of the PV system in this DC microgrid, a DC-DC boost converter is utilized. Fig. 4 illustrates the connection method of this equivalent circuit, consisting of an electronic power switch (IGBT), two capacitors, a diode, and an inductor.

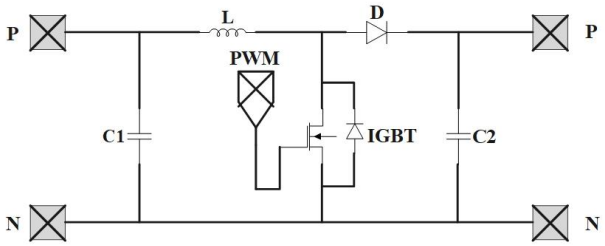

Fig. 4. Equivalent circuit of DC-DC boost converter.

The IGBT switch in this converter is controlled using the PWM method, with the switching signal generated by the MPPT control system.

3. Proposed Protection Scheme

In the effort to identify faults within DC microgrids, the proposed protection scheme relies on evaluating of apparent power, which includes both real and imaginary components. This methodology, involves simulating a variety of PP faults and PG faults with different fault resistances within the microgrid. Following this, current and voltage measurements are taken at relevant terminals to aid in fault identification, as detailed in [31].

By utilizing the Fourier transform, fault current and voltage can be transformed into the frequency domain, making it easier to extract frequency components from the faulted signals. This process involves using a sliding window technique, and the determination of frequency components is governed by the following mathematical relations:

$$I(k) = \frac{\sqrt{2}}{N} \sum_{n=0}^{N-1} i(n)\, e^{\frac{2\pi i n k}{N}} \tag{3}$$

$$V(k) = \frac{\sqrt{2}}{N} \sum_{n=0}^{N-1} v(n)\, e^{\frac{2\pi i n k}{N}} \tag{4}$$

In the above relations, N and k represent the number of samples and the Fourier spectrum index, respectively. Additionally, I(k) and V(k) represent the fault currents and voltages in the frequency domain [31].

The complex power in the frequency domain can be calculated by multiplying Eqs. (3) and (4), resulting in the following outcome:

$$S(k) = I(k) \cdot V(k) \tag{5}$$

Within the time domain, a sliding window methodology is employed to capture the frequency component and its temporal variations throughout the simulation period initiated by fault inception. This value is extracted within each sliding window, with each window consisting of a length of N=20 samples. The sliding window progresses forward by one sample throughout the simulation timeframe [31].

By analyzing the imaginary component of the apparent power, this approach facilitates the detection of faults. The imaginary component of the apparent power typically remains at zero during normal conditions, only deviating from this value when faults occur. As a result, it serves as a reliable indicator for fault detection. A predetermined threshold value is set for comparison with the imaginary component. If the imaginary component exceeds this threshold, a fault is detected:

$$\text{IFFT} = \text{Im}(S) \tag{6}$$

Numerous fault conditions, including both PP and PG faults, were tested at different fault resistances, ranging from low to high impedance faults. Additionally, the effectiveness of the proposed protection scheme was evaluated in Off-Grid and On-Grid scenarios. The results of these tests show the precise fault detection abilities of the proposed scheme. Fig. 5 illustrates the proposed protection algorithm through a block diagram representation [31].

3.1. Calculation of relay performance threshold

In order to identify the fault, the imaginary value of the apparent power is compared with a predetermined threshold value. This section will describe the steps for calculating the threshold value in offline mode:

The first step: Initially, PP and PG faults are simulated on every line connected to bus i, including various fault resistances, in both Off-Grid and On-Grid conditions. Subsequently, the highest IFFT value associated with each fault is computed and considered.

From this pool of values, the minimum is then selected for further analysis:

$$\min_{\psi}\left(\max(\text{IFFT}_{il})\right) \tag{7}$$

Second step: This process is repeated for each line linked to bus i, with the minimum IFFT value among all lines being designated as the threshold value (ξ) [31]. This threshold value is mathematically defined as follows:

$$\xi = \min_{\gamma}\left(\min_{\psi}\left(\max(\text{IFFT}_{il})\right)\right) \tag{8}$$

Ψ is a set of different faults in line l connected to bus i and γ is a set of faults in the whole DC microgrid [31].

Since the calculation steps for determining the threshold value are conducted at the control center, where access to the microgrid configuration is available, the threshold value can be accurately computed.

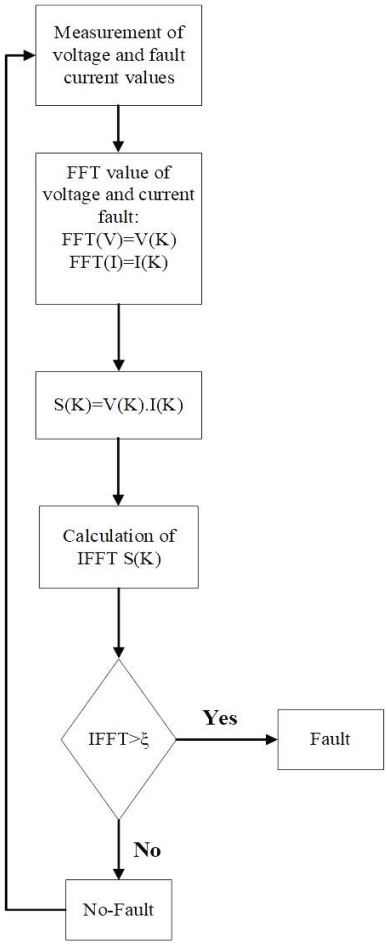

Fig. 5. Block diagram of the proposed protection algorithm.

3.2. Relay decision algorithm

Irrespective of the microgrid's state, whether On-Grid or Off-Grid, and regardless of the presence of high or low impedance faults, the relay decision algorithm operates according to the following principles:

Step A: Begin by measuring the pertinent voltage and current values.

Step B: Proceed to compute the frequency components of both voltage and current signals, subsequently determining the apparent power for these components.

Step C: Extract the imaginary component of the apparent power as decision value.

Step D: Utilize the aforementioned steps to calculate the threshold value, denoted as ξ.

Step E: Upon computation, compare the decision value with the threshold value ξ. If decision value exceeds ξ, a fault is identified within the DC microgrid.

3.3. Fault locating

To determine the location of the fault, as shown in Fig. 6, the first step is to measure the currents and voltages at the line terminals. In this process, the line model is simplified to a short model, taking into account the relevant resistance and inductance. The fault section, as illustrated in Fig. 6, is also considered.

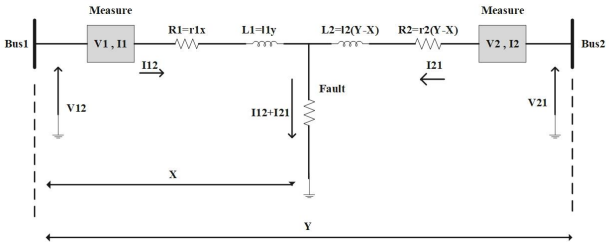

Fig. 6. Fault locating equivalent circuit.

The fault resistance denoted as R_f, as well as the resistance and inductance before the fault section represented by R_1 and L_1 respectively, along with the resistance and inductance after the fault section indicated as R_2 and L_2, two currents come into play [32]. The first one is the current flowing from Bus1 to the fault location is labeled as I_{12}, while the second one is the current from Bus2 to the fault location is denoted as I_{21} [31]. In light of these considerations, the voltages V_{12} and V_{21} can be computed as follows:

$$V_{12} = (r_1 + L_1\frac{dI_1}{dt})X + R_f(I_{12} + I_{21}) \tag{9}$$

$$V_{21} = (r_2 + L_2\frac{dI_2}{dt})(Y - X) + R_f(I_{12} + I_{21}) \tag{10}$$

The rate of change of current dI_1/dt and dI_2/dt is calculated as follows:

$$\frac{dI_1}{dt} = \frac{I_{12}(k) - I_{12}(k-1)}{T_s} \tag{11}$$

$$\frac{dI_2}{dt} = \frac{I_{21}(k) - I_{21}(k-1)}{T_s} \tag{12}$$

In this relation, T_s is the sampling interval and k is the sample number, so:

$$V_{12}(k) = \left[r_1 + L_1\left(\frac{I_{21}(k) - I_{21}(k-1)}{T_s}\right)\right]X + R_f\left(I_{12}(k) + I_{21}(k)\right) \tag{13}$$

$$V_{21}(k) = \left[r_2 + L_2\left(\frac{I_{12}(k) - I_{12}(k-1)}{T_s}\right)\right](Y - X) + R_f\left(I_{12}(k) + I_{21}(k)\right) \tag{14}$$

$$\begin{bmatrix} V_{12}(k) \\ V_{21}(k) - \left[r_2 + L_2\left(\frac{I_{12}(k)-I_{12}(k-1)}{T_s}\right)\right] Y \end{bmatrix} = \begin{bmatrix} J_{11} & J_{12} \\ J_{21} & J_{22} \end{bmatrix} \begin{bmatrix} X \\ R_f \end{bmatrix} \tag{15}$$

$$J_{11} = r_1 + L_1\left(\frac{I_{12}(k) - I_{12}(k-1)}{T_s}\right) \tag{16}$$

$$J_{12} = J_{22} = I_{12}(k) + I_{21}(k) \tag{17}$$

$$J_{21} = -r_2 - L_2\left(\frac{I_{21}(k) - I_{21}(k-1)}{T_s}\right) \tag{18}$$

In accordance with the subsequent equation, the value of X can be derived, representing fault location [32]:

$$[V] = [J][X] \tag{19}$$

$$[X] = [J^+][V] \tag{20}$$

$$J^+ = J^T\left(JJ^T\right)^{-1} \tag{21}$$

4. Simulation Results

In this section, the performance of DC microgrid protection under two scenarios, On-Grid and Off-Grid, has been examined, and the simulation results are as follows.

4.1. DC microgrid simulation results in On-Grid conditions

This section presents the proposed protective methodology and the simulation results for the microgrid shown in Fig. 1. Various fault scenarios, including PP and PG faults, have been simulated across a range of fault resistances, covering both high-impedance and low-impedance faults. These simulations were conducted in two distinct conditions: Off-Grid and On-Grid modes. The specifications of the microgrid in the On-Grid mode are detailed in Table 2.

Table 2. Microgrid parameters in On-Grid to the network.

Source	Current (A)	Voltage (V)	Power (W)
PV	11.63	677.98	**7855.62**
Battery	22.02	677.98	**14940.7**
Load	8.47	677.98	**5740.20**
PCC	25.23	677.98	**17056.1**

A) PP faults

PP faults are simulated on all buses with a fault resistance of 1Ω. The voltage and current profiles of the photovoltaic (PV) system, along with the corresponding IFFT plots and threshold values, are represented in Figs. 7 through 11.

Based on the conducted simulations, which included the aforementioned scenarios, the PP fault has been identified as the most critical fault type in DC microgrids. In each examined instance, the decision value exceeds the threshold value shortly after the fault occurs, resulting in rapid fault detection. Table 3 documents the highest decision value for each fault, along with the corresponding fault detection status and time. Analysis of this table reveals that all faults are detected within two milliseconds.

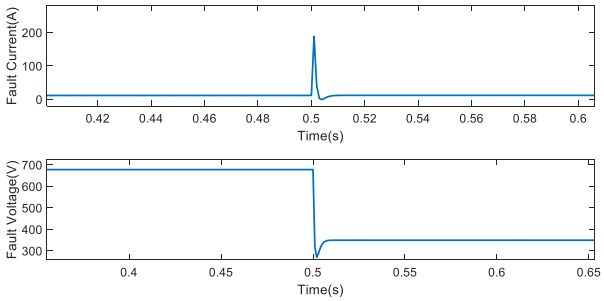

Fig. 7. PV current and voltage diagram under PP fault with 1Ω resistance.

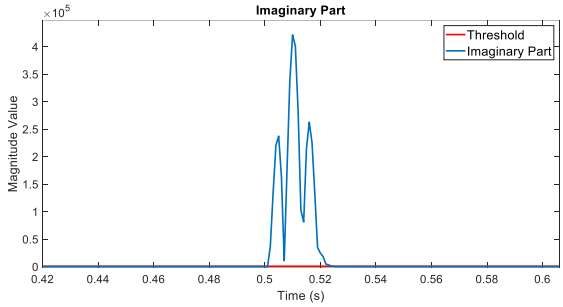

Fig. 8. Comparison threshold value and IFFT value related to PV under PP fault 1Ω resistance.

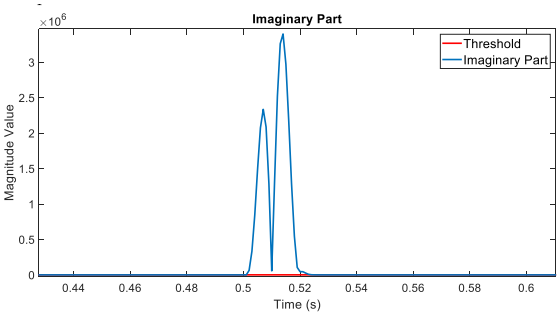

Fig. 9. Comparison threshold and IFFT value of PCC point PP fault 1Ω resistance.

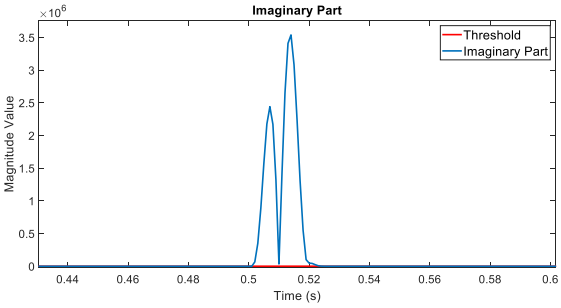

Fig. 10. Comparison threshold and IFFT value related to Load under PP fault 1Ω resistance.

B) PG fault

This section examines PG faults that occur in grid-connected mode, following the network specifications provided in Table 1. PG faults are simulated under both high impedance fault (HIF) and low impedance fault (LIF) conditions, using four different resistance values: 1Ω, 5Ω, 20Ω, and 40Ω. Figs. 12 to 15 illustrate the IFFT values compared to the threshold value for these simulations.

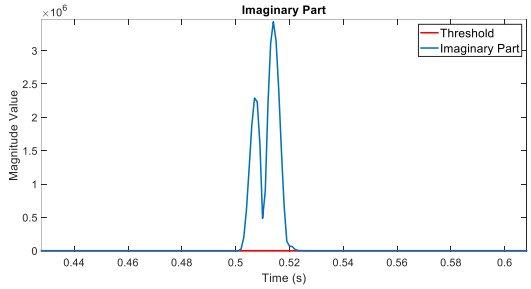

Fig. 11. Comparison threshold and IFFT value related to battery under PP fault 1Ω resistance.

Table 3. Examining the state of occurrence of faults in the DC microgrid in the state connected to the grid for PP faults.

DG	Fault resistance	Diagnosis	MAX_value (IFFT)	Fault detection time
PV	1Ω	Fault	4.2113×10^5	2ms
Battery	1Ω	Fault	3.4330×10^6	2ms
Load	1Ω	Fault	3.5392×10^6	2ms
PCC	1Ω	Fault	3.3986×10^6	2ms

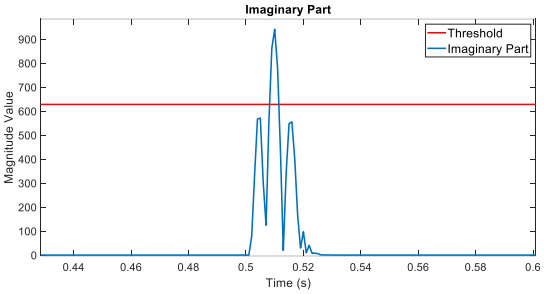

Fig. 12. Comparison threshold and IFFT value related to PV under PG fault 40Ω resistance.

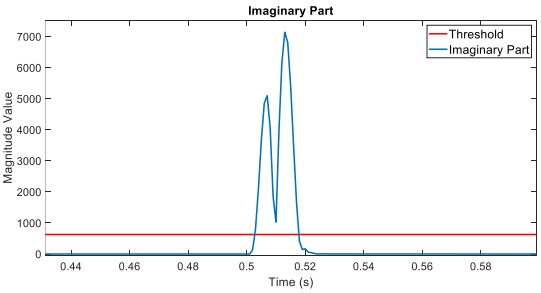

Fig. 13. Comparison threshold and IFFT value related to PCC under PG fault 40Ω resistance.

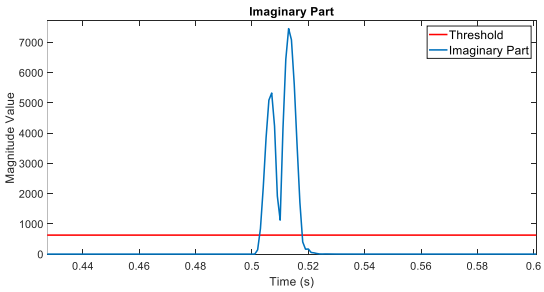

Fig. 14. Comparison threshold and IFFT value related to Load under PG fault 40Ω resistance.

As shown in the preceding figures, an analysis of PG faults was conducted under On-Grid conditions across various fault scenarios, with selected examples presented here. The results indicate that, in all fault instances, the IFFT value exceeds the threshold value, confirming the accurate fault identification by the relay decision algorithm. The characteristics of these faults, along with the comprehensive testing performed across all cases, are outlined in Table 4.

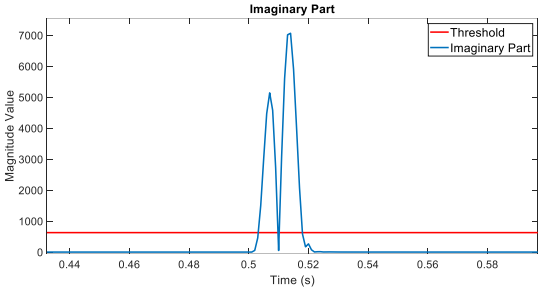

Fig. 15. Comparison threshold and IFFT value related to battery PG fault 40Ω resistance.

Table 4. Critical results of proposed algorithm for PG faults.

DG	Fault resistance	Fault detection	MAX_value (IFFT)	Fault detection time
PV	1Ω	Fault	4.0203×10^4	2ms
PV	5Ω	Fault	1.6451×10^4	2ms
PV	20Ω	Fault	2.9504×10^3	3ms
PV	40Ω	Fault	941.0751	9ms
Battery	1Ω	Fault	3.2419×10^5	2ms
Battery	5Ω	Fault	1.29×10^5	2ms
Battery	20Ω	Fault	2.2396×10^5	3ms
Battery	40Ω	Fault	7.0640×10^3	4ms
Load	1Ω	Fault	3.3639×10^5	2ms
Load	5Ω	Fault	1.3196×10^5	2ms
Load	20Ω	Fault	2.3401×10^4	3ms
Load	40Ω	Fault	7.4531×10^3	3ms
PCC	1Ω	Fault	3.2286×10^5	2ms
PCC	5Ω	Fault	1.2677×10^5	2ms
PCC	20Ω	Fault	2.2410×10^4	3ms
PCC	40Ω	Fault	7.1389×10^3	3ms

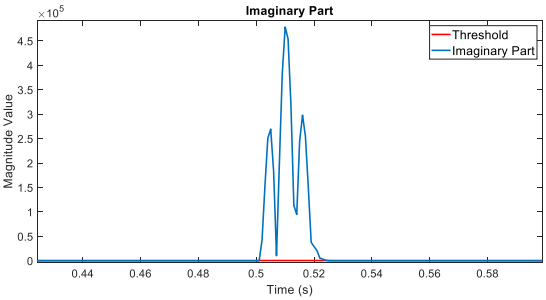

Fig. 16. Comparison threshold and IFFT value related to PV under PP fault with 1Ω resistance.

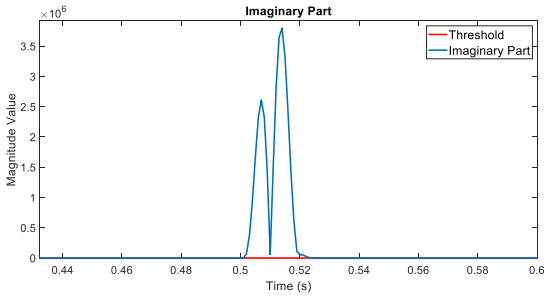

Fig. 17. Comparison threshold and IFFT value related to Load under PP fault 1Ω resistance.

Table 5. Microgrid parameters in Off-Grid mode.

Source	Current (A)	Voltage (V)	Power (W)
PV	11.61	702.82	**8154.17**
Battery	-2.82	702.82	**-1985.11**
Load	8.78	702.82	**6179.87**
PCC	0	702.82	**0**

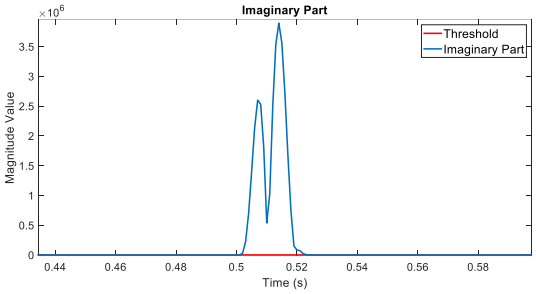

Fig. 18. Comparison threshold and IFFT value related to battery under PP fault 1Ω resistance.

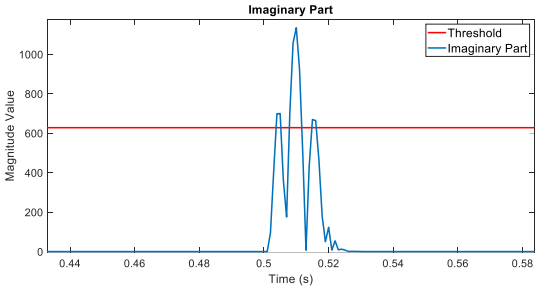

Fig. 19. Comparison threshold and IFFT value related to PV under PG fault 40Ω resistance.

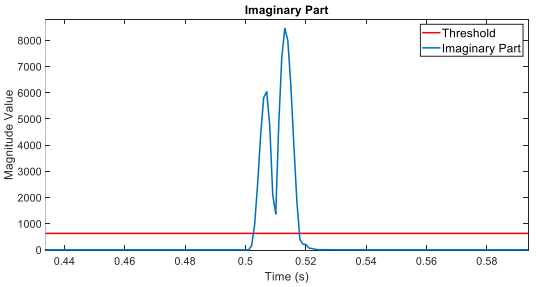

Fig. 20. Comparison threshold and IFFT value related to Load PG fault with 40Ω resistance.

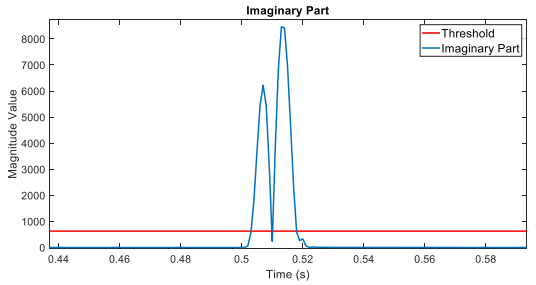

Fig. 21. Comparison threshold and IFFT value related to battery PG fault 40Ω resistance.

Table 6. Simulation results of DC microgrid in Off-Grid mode for PP faults.

DG	Fault Resistance	Fault Detection	MAX_Value (IFFT)	Fault Detection Time
PV	1Ω	Fault	4.7847×10^5	2ms
Battery	1Ω	Fault	3.8914×10^6	2ms
Load	1Ω	Fault	3.7965×10^6	2ms

Table 7. Simulation results of DC microgrid in Off-Grid mode for PG faults.

DG	Fault resistance	Diagnosis	MAX_value (IFFT)	Fault detection time
PV	1Ω	Fault	4.7814×10^4	2ms
PV	5Ω	Fault	1.9681×10^4	2ms
PV	20Ω	Fault	3.5493×10^3	3ms
PV	40Ω	Fault	1.1342×10^3	4ms
Battery	1Ω	Fault	3.8275×10^5	2ms
Battery	5Ω	Fault	1.5302×10^5	2ms
Battery	20Ω	Fault	2.6677×10^4	3ms
Battery	40Ω	Fault	8.4639×10^3	4ms
Load	1Ω	Fault	3.7491×10^5	2ms
Load	5Ω	Fault	1.4792×10^5	2ms
Load	20Ω	Fault	2.6503×10^4	3ms
Load	40Ω	Fault	8.4570×10^3	3ms

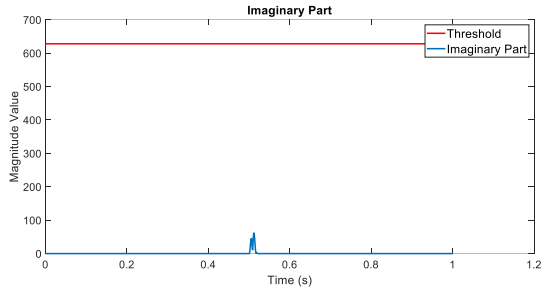

Fig. 22. Comparison IFFT value and threshold value in condition of PV interruption.

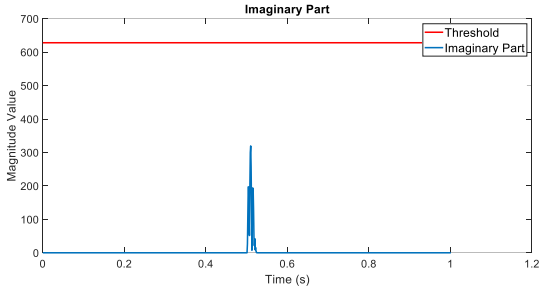

Fig. 23. Comparison IFFT value and threshold value in condition of load interruption.

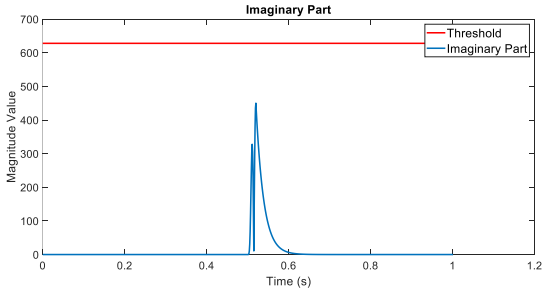

Fig. 24. Comparison IFFT value and threshold value in condition of battery disconnection.

4.2. Simulation results of DC microgrid in Off-Grid condition

Table 5 displays the specifications of the microgrid in Off-Grid mode. In this section, simulation results for the proposed approach

Table 8. Fault location results of the studied microgrid per PP fault.

DG	r_1 (Ω)	l_1 (mH)	r_2 (Ω)	l_2 (mH)	X (m)
PV	0.5	0.5	0.5	0.5	501.6078
PV	0.3	0.3	0.7	0.7	301.6763
PV	0.7	0.7	0.3	0.3	702.7546
Battery	0.5	0.5	0.5	0.5	480.2133
Battery	0.3	0.3	0.7	0.7	273.3498
Battery	0.7	0.7	0.3	0.3	691.1231
Load	0.5	0.5	0.5	0.5	499.7843
Load	0.3	0.3	0.7	0.7	300.2168
Load	0.7	0.7	0.3	0.3	699.1845

Table 9. Fault location results of the studied microgrid per PG fault.

DG	r_1 (Ω)	l_1 (mH)	r_2 (Ω)	l_2 (mH)	X (m)
PV	0.5	0.5	0.5	0.5	543.9570
PV	0.3	0.3	0.7	0.7	355.2380
PV	0.7	0.7	0.3	0.3	729.4199
Battery	0.5	0.5	0.5	0.5	479.0217
Battery	0.3	0.3	0.7	0.7	261.1846
Battery	0.7	0.7	0.3	0.3	691.5214
Load	0.5	0.5	0.5	0.5	484.9524
Load	0.3	0.3	0.7	0.7	287.2515
Load	0.7	0.7	0.3	0.3	687.4691

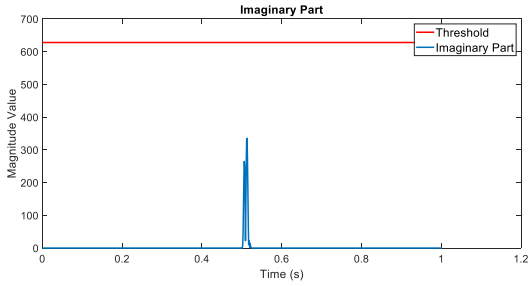

Fig. 25. Comparison of IFFT value and threshold value in PCC cutoff condition.

in the case of Off-Grid mode are presented.

A) PP fault

PP faults were simulated on all buses with a fault resistance of 1Ω. The corresponding plots comparing the IFFT results and threshold values are shown in Figs. 16-18.

Based on the simulation results, as shown in the figures mentioned above, it is observed that in every case of PP faults, the IFFT exceeds the threshold value shortly after the fault initiation, resulting in prompt fault detection. Table 6 presents details on the highest IFFT value for each fault, as well as the corresponding fault detection status and detection time. Moreover, an analysis of this table confirms that all faults are detected within 2 milliseconds.

B) PG fault

This section of the study focuses on simulating PG faults in Off-Grid mode, in accordance with the network specifications outlined in Table 6. PG faults are analyzed across both HIF and LIF, with simulations carried out using four different resistor values: 1Ω, 5Ω, 20Ω, and 40Ω. Furthermore, comparative graphs illustrating the IIFFT and threshold values can be found in Figs. 19 to 21.

The analysis of the provided figures indicates that PG faults were investigated under Off-Grid conditions across different fault scenarios, with specific examples highlighted. The investigations show that in all fault cases, the IFFT value exceeds the threshold value, allowing for the precise detection of faults by the relay decision algorithm. Detailed characteristics of these faults, as well as the tests conducted in all scenarios, are documented in Table 7.

4.3. Fault location

This section investigates into the fault location using the concept of an equivalent circuit, as shown in Fig. 6. Due to the short length of the lines in this DC microgrid, they are represented as combinations of resistances and inductances. For simulation purposes, specific parameters are used: R=1Ω, L=1mH, and a distance of 1000m between the local and remote terminals of the line (Y). To evaluate the effectiveness of the location algorithm, simulations are conducted with fault locations varied at 30%, 50%, and 70% of the total line length. The simulations include both PP and PG faults at specific locations, with the results presented in Tables 8 and 9, demonstrating the algorithm's robust performance.

In these tables, r_1 and l_1 indicate the resistance and inductance of the line between the local terminal and the fault location, while r_2 and l_2 represent the resistance and inductance of the line between the remote terminal and the fault location. Additionally, X signifies the fault location.

4.4. Performance of protection scheme in case of topology change

After conducting thorough investigations within the examined microgrid, the intended protection plan has been successfully implemented, requiring a modification in the microgrid's topology. Instances where the Load, PV, and Battery are completely disconnected from the circuit, along with subsequent measurements and the determination of the IFFT value followed by its comparison to the threshold value, reveal that in such scenarios, the IFFT value falls below the threshold value, resulting in the detection of no fault condition. Therefore, it can be concluded that the proposed algorithm operates effectively. Furthermore, the efficacy of the proposed algorithm has been validated under conditions such as PCC disconnection and transitioning of the microgrid to Off-Grid mode. Importantly, the algorithm functions as intended in these scenarios, with no faults detected. Figs. 22 to 25 depict the comparison between IFFT and the threshold value, consistently showing instances where the IFFT remains below the threshold value, leading to the absence of fault detection.

5. Conclusion and Future Work

The proposed methodology utilizes IFFT to detect faults within the DC microgrid by comparing the IFFT values to a predefined relay threshold. This allows for fault detection based on the magnitude of the IFFT value, effectively addressing PP and PG faults and demonstrating robust performance in both microgrid operation modes. The protection scheme accurately identifies High-Impedance Faults (HIF) and Low-Impedance Faults (LIF) across a resistance range of 0 to 50 ohms. Changes in microgrid topology do not impact the determination of the relay threshold value, ensuring the reliable operation of the protective relays. The proposed method excels at fault localization by pinpointing fault locations based on varying impedances. The proposed approach efficiently identifies PP and PG faults, including high-impedance faults up to 50 ohms, within 2-3 milliseconds in both grid-connected and islanded modes while ensuring precise fault location with minimal error across different positions.

Moving forward, future research could explore the possibility of adaptive threshold value calculation, enabling dynamic adjustment of threshold values in response to changing network conditions. The integration of cumulative protection strategies shows promise in enhancing fault detection capabilities. Additionally, refining the protective algorithm to differentiate between fault modes and accurately identify fault types represents a crucial area for further development. These advancements are expected to significantly improve the effectiveness and versatility of fault detection mechanisms in DC microgrid systems.

REFERENCES

[1] F. S. Al-Ismail, "Dc microgrid planning, operation, and control: A comprehensive review," *IEEE Access*, vol. 9, pp. 36154–36172, 2021.

[2] M. Zolfaghari, G. B. Gharehpetian, M. Shafie-khah, and J. P. Catalão, "Comprehensive review on the strategies for controlling the interconnection of ac and dc microgrids," *Int. J. Electr. Power Energy Syst.*, vol. 136, p. 107742, 2022.

[3] V. F. Pires, A. Pires, and A. Cordeiro, "Dc microgrids: benefits, architectures, perspectives and challenges," *Energies*, vol. 16, no. 3, p. 1217, 2023.

[4] M. Shirkhani, J. Tavoosi, S. Danyali, A. K. Sarvenoee, A. Abdali, A. Mohammadzadeh, and C. Zhang, "A review on microgrid decentralized energy/voltage control structures and methods," *Energy Rep.*, vol. 10, pp. 368–380, 2023.

[5] M. Mola, A. Afshar, N. Meskin, and M. Karrari, "Distributed fast fault detection in dc microgrids," *IEEE Syst. J.*, vol. 16, no. 1, pp. 440–451, 2020.

[6] Z. Ali, Y. Terriche, S. Z. Abbas, M. A. Hassan, M. Sadiq, C.-L. Su, and J. M. Guerrero, "Fault management in dc microgrids: A review of challenges, countermeasures, and future research trends," *IEEE Access*, vol. 9, pp. 128032–128054, 2021.

[7] B. Zareinia, A. R. Ghiasi, and M. A. Badamchizadeh, "A new integrated fault detection and control scheme of islanded dc microgrids: A resilient approach," *ISA Trans.*, vol. 146, pp. 165–174, 2024.

[8] A. Deb and A. K. Jain, "An effective data-driven machine learning hybrid approach for fault detection and classification in a standalone low-voltage dc microgrid," *Electr. Eng.*, 2024.

[9] I. Grcic, H. Pandzic, and D. Novosel, "Fault detection in dc microgrids using short-time fourier transform," *Energies*, vol. 14, no. 2, p. 277, 2021.

[10] A. H. Poursaeed and F. Namdari, "High-speed algorithm for fault detection and location in dc microgrids based on a novel time–frequency analysis," *IET Gener. Transm. Distrib.*, 2024.

[11] N.-C. Yang and J.-M. Yang, "Fault classification in distribution systems using deep learning with data preprocessing methods based on fast dynamic time warping and short-time fourier transform," *IEEE Access*, vol. 11, pp. 63612–63622, 2023.

[12] A. Ezzat, B. E. Elnaghi, and A. A. Abdelsalam, "Microgrids islanding detection using fourier transform and machine learning algorithm," *Electr. Power Syst. Res.*, vol. 196, p. 107224, 2021.

[13] D. K. Asl, A. Hamedi, M. Shadaei, H. Samet, and T. Ghanbari, "A non-iterative method based on fast fourier transform and least square for fault locating in dc microgrids," in *2020 IEEE Int. Conf. Environ. Electr. Eng.*, pp. 1–5, IEEE, 2020.

[14] A. R. Aqamohammadi, T. Niknam, S. Shojaeiyan, P. Siano, and M. Dehghani, "Deep neural network with hilbert–huang transform for smart fault detection in microgrid," *Electron.*, vol. 12, no. 3, p. 499, 2023.

[15] A. Cano, P. Arévalo, D. Benavides, and F. Jurado, "Integrating discrete wavelet transform with neural networks and machine learning for fault detection in microgrids," *Int. J. Electr. Power Energy Syst.*, vol. 155, p. 109616, 2024.

[16] M. Zakir, A. Arshad, H. A. Sher, and A. Al-Durra, "Design and implementation of a fault detection method for a pv-fed dc-microgrid with power control mechanism," *IET Electr. Power Appl.*, vol. 16, no. 9, pp. 1057–1071, 2022.

[17] H. L. Dang, S. Kwak, and S. Choi, "Advanced learning technique based on feature differences of moving intervals for detecting dc series arc failures," *Mach.*, vol. 12, no. 3, p. 167, 2024.

[18] R. Montoya, B. P. Poudel, A. Bidram, and M. J. Reno, "Dc microgrid fault detection using multiresolution analysis of traveling waves," *Int. J. Electr. Power Energy Syst.*, vol. 135, p. 107590, 2022.

[19] N. Bayati, H. R. Baghaee, A. Hajizadeh, M. Soltani, and Z. Lin, "Mathematical morphology-based local fault detection in dc microgrid clusters," *Electr. Power Syst. Res.*, vol. 192, p. 106981, 2021.

[20] G. K. Rao and P. Jena, "Fault detection in dc microgrid based on the resistance estimation," *IEEE Syst. J.*, vol. 16, no. 1, pp. 1009–1020, 2021.

[21] N. Bayati, H. R. Baghaee, M. Savaghebi, A. Hajizadeh, M. Soltani, and Z. Lin, "Emd/ht-based local fault detection in dc microgrid clusters," *IET Smart Grid*, vol. 5, no. 3, pp. 177–188, 2022.

[22] E. N. Prasad and P. K. Dash, "Fault analysis in photovoltaic generation based dc microgrid using multifractal detrended fluctuation analysis," *Int. Trans. Electr. Energy Syst.*, vol. 31, no. 1, p. e12564, 2021.

[23] R. Peña-Alzola, M. Sztykiel, C. E. Jones, P. J. Norman, G. Moore, J. Pou, and G. M. Burt, "First-fault detection in dc distribution with it grounding based on sliding discrete fourier-transform," *IEEE Trans. Power Electron.*, vol. 36, no. 4, pp. 3649–3654, 2020.

[24] S. Salehimehr, S. M. Miraftabzadeh, and M. Brenna, "A novel machine learning-based approach for fault detection and location in low-voltage dc microgrids," *Sustainability*, vol. 16, no. 7, p. 2821, 2024.

[25] M. Ahmadipour, M. M. Othman, R. Bo, Z. Salam, H. M. Ridha, and K. Hasan, "A novel microgrid fault detection and classification method using maximal overlap discrete wavelet packet transform and an augmented lagrangian particle swarm optimization-support vector machine," *Energy Rep.*, vol. 8, pp. 4854–4870, 2022.

[26] L. Kong and H. Nian, "Fault detection and location method for mesh-type dc microgrid using pearson correlation coefficient," *IEEE Trans. Power Deliv.*, vol. 36, no. 3, pp. 1428–1439, 2020.

[27] Z. Rafiee, S. Hajiaghasi, M. Rafiee, and A. Salemnia, "A new method for analysis and estimation of microgrid signals under fault conditions," *J. Control Autom. Electr. Syst.*, vol. 32, pp. 1099–1110, 2021.

[28] A. Ameli, K. A. Saleh, A. Kirakosyan, E. F. El-Saadany, and M. M. Salama, "An intrusion detection method for line current differential relays in medium-voltage dc microgrids," *IEEE Trans. Inf. Forensics Secur.*, vol. 15, pp. 3580–3594, 2020.

[29] Y. Xia, F. Yu, X. Xiong, Q. Huang, and Q. Zhou, "A novel microgrid islanding detection algorithm based on a multi-feature improved lstm," *Energies*, vol. 15, no. 8, p. 2810, 2022.

[30] E. Igbineweka and S. Chowdhury, "Application of dual-tree complex wavelet transformation in islanding detection for a hybrid ac/dc microgrid with multiple distributed generators," *Energies*, vol. 17, no. 20, p. 5133, 2024.

[31] S. K. Prince, S. Affijulla, and G. Panda, "Protection of dc microgrids based on complex power during faults in on/off-grid scenarios," *IEEE Trans. Ind. Appl.*, vol. 59, no. 1, pp. 244–254, 2022.

[32] P. Chauhan, C. Gupta, and M. Tripathy, "High speed fault detection and localization scheme for low voltage dc microgrid," *Int. J. Electr. Power Energy Syst.*, vol. 146, p. 108712, 2023.